Intensities of electronic Raman scattering between crystal-field levels of Ce^{3+} in $LuPO_4$: Nonresonant and near-resonant excitation

G. M. Williams,* P. C. Becker,† J. G. Conway, and N. Edelstein
Department of Physics, University of California, Berkeley, California 94720
and Materials and Chemical Sciences Division, Lawrence Berkeley Laboratory, 1 Cyclotron Road, Berkeley, California 94720

L. A. Boatner and M. M. Abraham
Solid State Division, Oak Ridge National Laboratory, P.O. Box 2008, Oak Ridge, Tennessee 37831-6032
(Received 16 January 1989)

The relative intensities of the electronic Raman scattering between individual crystal-field states of the $4f^1$ configuration of Ce^{3+} in $LuPO_4$ are compared to those calculated with use of the standard second-order theory, and also by explicitly evaluating the sum over the virtual intermediate states using the crystal-field wave functions and observed energies of the $5d^1$ configuration. The results show that the explicit calculation predicts the observed relative intensities much more accurately than the standard theory. In addition, a change in the incident laser energy from the argon-ion green line (514.5 nm) to that of the frequency-tripled output of a Nd^{3+}:YAG (355 nm) laser results in enhancements of the electronic Raman scattering intensities by factors on the order of 100. These enhancements are accurately predicted by the explicit calculation.

I. INTRODUCTION

Electronic Raman scattering is a two-photon process in which one photon is provided by the laser field and the second is generated spontaneously from the vacuum. The standard second-order theory of $4f^N$-$4f^N$ two-photon transitions developed by Axe[1] closely follows the Judd-Ofelt theory[2,3] for the intensities of the formally parity-forbidden $4f^N$-$4f^N$ one-photon transitions. Both calculations include summations over the states belonging to excited electronic configurations of the rare-earth ion whose parity is opposite that of the ground f^N configuration. The sums are greatly reduced by the closure approximation, which assumes the states of any given excited configuration are degenerate in energy. The result, in both cases, is that only a limited number of parameters is needed to describe the relative intensities for all the transitions in a given crystal. The two-photon experiments serve as a more stringent test of the closure approximation, however, because of the reduced number of parameters needed to describe the parity-allowed two-photon transitions.

Recently, the relative cross sections for two-photon absorption transitions between the Russell-Saunders multiplets of Eu^{2+} and Gd^{3+} (both $4f^7$ systems) have been studied.[4–6] In general, the observed relative cross sections agreed well with the standard theory. A number of transitions with $\Delta J > 2$, $\Delta L > 2$, or $\Delta S \neq 0$, were observed, however. These transitions are forbidden by the standard second-order theory. To adequately account for these forbidden transitions, higher-order perturbation theory was utilized allowing the spin-orbit and crystal-field interactions to mix states in the opposite-parity configurations[7]—in essence, adding more detail to the form of the intermediate states.

Subsequently, we compared the observed and calculated relative intensities of electronic Raman transitions between crystal-field levels of Er^{3+} ($4f^{11}$) and Tm^{3+} ($4f^{12}$) in crystals of $ErPO_4$ and $TmPO_4$, respectively.[8] The agreement between experiment and theory was adequate for Er^{3+}, but serious discrepancies existed for Tm^{3+}. Usually, it is assumed that the predominant intermediate states arise from the $4f^{N-1}5d$ configuration, which is closest in energy to the ground $4f^N$ configuration. Subsequently, it was shown that the Tm^{3+} results could be explained by a mechanism in which intermediate states with g-orbital characteristics contribute equally with the d-orbital states to the intensities.[9] This is not such a surprising result if one considers the intermediate state to be not atomiclike states of the rare-earth ion, but rather to be molecularlike states of the rare-earth ion and the surrounding ligands. Such a molecular orbital is just as likely to have g-orbital character as d-orbital character.[9,10]

Ce^{3+} has a unique electronic structure that makes it an interesting case for electronic Raman scattering studies. The two important features are as follows. (1) Ce^{3+} has only one optically active $4f$ electron. This lends simplicity to all of the calculations and reduces the number of physical interactions that may contribute to the electronic Raman scattering process. (2) Ce^{3+}, relative to the other trivalent rare-earth ions, has a first-excited configuration ($5d^1$) that is rather low in energy. For Ce^{3+} in $LuPO_4$ the states of the $5d^1$ configuration span the range from 30 000 to 50 000 cm^{-1}. This low energy of the first-excited configuration makes Ce^{3+} an especially stringent test of the closure approximation used in the standard electronic Raman scattering theory.

We report in this paper an electronic Raman investigation of Ce^{3+} in $LuPO_4$. The results were used to locate and determine the symmetries of all the states associated with the $4f^1$ configuration of Ce^{3+}. The energies of the $5d^1$ configuration have been determined from optical-absorption measurements. The experimental energy levels were fitted with the appropriate Hamiltonians, and wave functions for the levels have been obtained. From this information, the measured relative intensities of the electronic Raman transitions were compared to the values calculated in two ways: using the standard theory, and by the explicit evaluation of the sum over the states of the $5d^1$ configuration.

Another consequence of the low energy of the first-excited configuration is that it permits near-resonant excitation of a parity-allowed transition in order to enhance the electronic Raman scattering. In most rare-earth-doped crystals, the transitions accessible by lasers are between states of the ground $4f^N$ configuration. For such intraconfigurational resonances, the enhancements of the electronic Raman process are, in general, found to be quite small[11–15] because the $4f^N$-$4f^N$ electric dipole matrix elements determining the strength of the resonance are formally parity forbidden. For the case of Ce^{3+} in $LuPO_4$, the frequency-tripled output of a Nd^{3+}:YAG laser (YAG denotes yttrium aluminum garnet) at 355 nm (28 191.5 cm^{-1}) is in near resonance with the transition between the $4f^1$ ground state and the lowest-energy state of the $5d^1$ configuration at approximately 30 000 cm^{-1}. We report the observation of near-resonance enhancements of the electronic Raman scattering intensities on the order of 100 (including the enhancement due to the usual ω^4 scattering dependence) for laser excitation at 355 nm (28 191.5 cm^{-1}) relative to laser excitation at 514.5 nm (19 429.7 cm^{-1}). These enhancements are accurately described by a calculation in which the sum is performed explicitly over the states of the $5d^1$ configuration.

II. EXPERIMENT

The samples used in the experiments were single crystals of Ce^{3+}:$LuPO_4$. $LuPO_4$ is an insulating crystal with a band gap in the vacuum ultraviolet (at about 70 000 cm^{-1}).[16] It is uniaxial with a tetragonal zircon structure (space group D_{4h}^{19}).[17] In the Ce^{3+}:$LuPO_4$ crystals, cerium ions replace some fraction of the lutetium ions. High doping levels of Ce^{3+} are preferred in order to observe the inherently weak electronic Raman scattering signal. At sufficiently high cerium concentrations, however, the structure of the crystal changes from the tetragonal phase to the lower-symmetry monoclinic phase found for $CePO_4$. The crystals used in this experiment were selected from batches in which the starting materials contained a 20 mol % concentration of cerium relative to lutetium.[18] A typical crystal selected for the study was a platelet with dimensions 15 mm×4 mm×1 mm that had the tetragonal structure of $LuPO_4$.

All the electronic Raman scattering spectra were taken with a 90° scattering geometry. Light was incident along one of the two equivalent crystal axes, $\hat{\mathbf{X}}$, and the scattered light was collected along the other equivalent axis, $\hat{\mathbf{Y}}$. Spectra were obtained for four different combinations of scattered (first Cartesian coordinate) and incident (second Cartesian coordinate) polarizations, $\hat{\mathbf{X}}\hat{\mathbf{Y}}$, $\hat{\mathbf{Z}}\hat{\mathbf{Z}}$, and $\hat{\mathbf{Z}}\hat{\mathbf{Y}}$.

The nonresonant electronic Raman spectra were excited with the 514.5-nm (19 429.7 cm^{-1}), 488.0-nm (20 486.7 cm^{-1}), and 457.9-nm (21 831.0 cm^{-1}) lines of a cw argon-ion laser. None of these lines are near any electronic states of the cerium ion. After correction for the ω^4 scattering dependence and the spectral characteristics of the experimental apparatus, all three excitation frequencies yielded the same spectra within the experimental uncertainty. The observed scattering intensities described in Sec. IV were all taken from runs using the 514.5-nm laser line. The results were averaged over several runs using several different crystals. All scattering experiments were performed at temperatures of approximately 10–15 K. Details of the experimental setup have been described previously.[8]

The near-resonant electronic Raman spectra were excited by the tripled output of a Quanta-Ray (DCR1 Q-switched Nd^{3+}:YAG laser operated at a 10-Hz repetition rate. The output was at 355 nm (28 191.5 cm^{-1}). The polarization of the laser could be rotated by 90° by insertion of a half-wave plate. All lenses used in the experiment were made of ultraviolet-transmitting Suprasil quartz. The laser was focused onto the sample by a 15-cm-focal-length lens. Pulse energies above approximately 0.3 mJ, in conjunction with the tightest possible focusing using the 15-cm lens, resulted in visible pitting of the crystal. All measurements were taken with the laser intensity less than this damage threshold. The scattered light was collected at 90° by a 5-cm-focal-length lens and then focused onto the slit of a Spex Industries, Inc. 1403 double monochromator by a 30-cm-focal-length lens. Before entering the monochromator, a single polarization was selected by a Glan-Thompson prism polarizer. After spectral analysis by the monochromator, the scattered photons were detected by a RCA C31034 photomultiplier tube. Care was taken to ensure that the signal strength did not saturate the photomultiplier tube. The resulting current pulse was immediately passed through a LeCroy Corporation 100B×10 current amplifier before being detected by a Stanford Research Systems, Inc. SRS-250 gated integrator. The integrator was used as a single-shot, sample-and-hold device with the signal from each shot being digitized by a 12-bit analog-to-digital (A/D) converter and stored on a Digital Equipment Corporation LSI11/2 microcomputer. One-hundred laser shots were averaged for each data point. The LSI11/2 computer was also used to control the monochromator. In order to compare the electronic Raman scattering intensities from 355-nm excitation to those from 514.5-nm excitation, a normalization procedure was employed. The vibrational scattering from the crystal phonons should be independent of excitation energy other than normal ω^4-type dependence. This is valid under the usual assumption that the lattice vibrations of the crystal are not strongly coupled to the $4f$ electronic states of the rare-earth ion. For each experiment, the electronic Raman

scattering intensities were normalized by scaling the results relative to the intensity of the Raman scattering transition involving the 1034-cm^{-1} E_g phonon of the crystal. This not only corrects for differences between the two experiments (i.e., laser power, frequency response of the detection system, etc.), but also corrects for enhancements resulting from the ω^4-type scattering dependence.

Low-resolution (on the order of 10 cm^{-1}) absorption spectra of the $5d^1$ configuration were obtained using a Cary 17 spectrophotometer. The spectrometer was purged with dry N_2 gas to allow operation below 200 nm. Spectra were taken at 295, 77, and 10 K.

High-resolution absorption spectra were obtained with an experimental setup employing a 30-W D_2 lamp as an ultraviolet-light source and the Spex 1403 double monochromator as the spectral analyzer. It was necessary to use the Spex 1403 in second order since it does not operate above 30 000 cm^{-1} in first order. Colored glass filters were used to eliminate the visible light from the D_2 source. A near-ultraviolet transmitting-sheet polarizer or a Glan-Thompson prism polarizer was used as a polarization analyzer. The resolution of the system was approximately 1 cm^{-1}, and the operating range was from 30 000 to 43 000 cm^{-1}.

III. ELECTRONIC STRUCTURE

A. The lowest-energy configuration, $4f^1$

Spin-orbit coupling is the largest interaction affecting the $4f^1$ configuration and splits the configuration into two multiplets, $^2F_{5/2}$ and $^2F_{7/2}$, separated by approximately 2200 cm^{-1}. These levels are further split by the crystal field of the $LuPO_4$ crystal host. The point-group symmetry of the crystal field about the cerium ion is D_{2d}. The crystal-field levels are labeled by the irreducible representations of the double group of D_{2d}, Γ_6 and Γ_7. Each of these levels is a Kramers doublet.

Nakazawa and Shionoya[19] used the strong parity-allowed $4f^1$-$5d^1$ luminescence and absorption spectra to locate five out of the seven $4f^1$ levels. In the present work, electronic Raman scattering originating from the ground state was used to locate all seven levels. Some typical electronic Raman spectra are shown in Fig. 1. The $4f^1$ energy-level structure is shown in Fig. 2. Symmetry assignments were made based on the electronic Raman scattering selection rules:[20] For $\hat{\mathbf{X}}\hat{\mathbf{Y}}$, $\hat{\mathbf{X}}\hat{\mathbf{Z}}$, and $\hat{\mathbf{Z}}\hat{\mathbf{Y}}$,

$$\begin{aligned} &\Gamma_6 \rightarrow \Gamma_6 \text{ or } \Gamma_7 , \\ &\Gamma_7 \rightarrow \Gamma_6 \text{ or } \Gamma_7 , \end{aligned} \tag{1}$$

and for $\hat{\mathbf{Z}}\hat{\mathbf{Z}}$,

$$\begin{aligned} &\Gamma_6 \rightarrow \Gamma_6 , \\ &\Gamma_7 \rightarrow \Gamma_7 , \end{aligned} \tag{2}$$

where the Cartesian coordinates refer to the polarization of the scattered photon and the incident laser photon, respectively.

The spin-orbit and crystal-field parameters of a semiempirical Hamiltonian were obtained by fitting the calculated energies to the observed energy levels. The wave functions obtained from these fitted parameters are essential to the electronic Raman scattering intensity calculations and are listed in Table I.

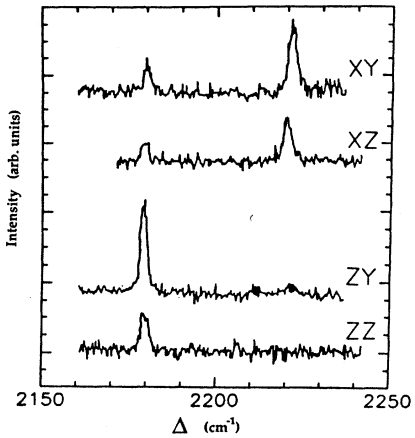

FIG. 1. Example of an electronic Raman spectrum of a nominally 20% Ce^{3+} in $LuPO_4$ crystal excited by the 514.5-nm line of an argon-ion laser. The temperature was approximately 10 K.

The Hamiltonian used is of the form

$$H = H_{\text{spin orbit}} + H_{\text{crystal field}} , \tag{3}$$

where

$$H_{\text{spin orbit}} = \zeta_f(\mathbf{s}\cdot\mathbf{l}) , \tag{4}$$

$$\begin{aligned} H_{\text{crystal field}} = {} & B_0^2 C_0^2 + B_0^4 C_0^4 \\ & + B_4^4 (C_4^4 + C_{-4}^4) + B_0^6 C_0^6 \\ & + B_4^6 (C_4^6 + C_{-4}^6) , \end{aligned} \tag{5}$$

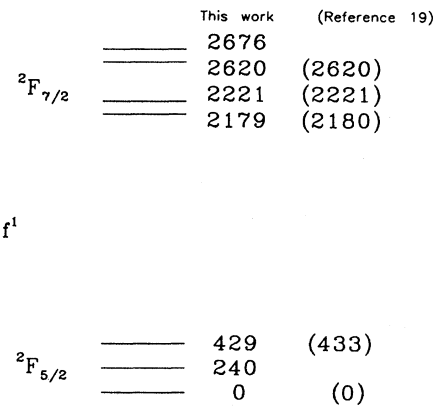

FIG. 2. Energy levels for the $4f^1$ configuration of Ce^{3+} in $LuPO_4$. For this work, the mole fraction of cerium ions was nominally 20%. For Ref. 19, the mole fraction was approximately 0.1%.

TABLE I. Wave functions for the $4f^1$ configuration of Ce^{3+} in crystals of nominally 20% Ce^{3+} in $LuPO_4$.

Energy (cm^{-1})	Symmetry	Wave function $\sum_{J,J_z} a(J,J_z)^{2S+1}L\|J,J_z\rangle$
0.0	Γ_6	$0.749\,^2F\|\frac{5}{2},-\frac{3}{2}\rangle+0.658\,^2F\|\frac{5}{2},\frac{5}{2}\rangle$
240.0	Γ_7	$0.991\,^2F\|\frac{5}{2},-\frac{1}{2}\rangle-0.103\,^2F\|\frac{7}{2},-\frac{1}{2}\rangle$
429.0	Γ_6	$-0.749\,^2F\|\frac{5}{2},\frac{5}{2}\rangle+0.651\,^2F\|\frac{5}{2},-\frac{3}{2}\rangle+0.113\,^2F\|\frac{7}{2},-\frac{3}{2}\rangle$
2179.0	Γ_6	$-0.867\,^2F\|\frac{7}{2},\frac{5}{2}\rangle-0.484\,^2F\|\frac{7}{2},-\frac{3}{2}\rangle+0.117\,^2F\|\frac{5}{2},-\frac{3}{2}\rangle$
2221.0	Γ_7	$0.756\,^2F\|\frac{7}{2},-\frac{1}{2}\rangle+0.653\,^2F\|\frac{7}{2},\frac{7}{2}\rangle$
2620.0	Γ_7	$0.753\,^2F\|\frac{7}{2},\frac{7}{2}\rangle-0.645\,^2F\|\frac{7}{2},-\frac{1}{2}\rangle-0.131\,^2F\|\frac{5}{2},-\frac{1}{2}\rangle$
2676.0	Γ_6	$-0.868\,^2F\|\frac{7}{2},-\frac{3}{2}\rangle+0.491\,^2F\|\frac{7}{2},\frac{5}{2}\rangle$

and ζ_f and the B_q^k's are treated as parameters.

The fit was made to seven energy levels using six parameters. In general, the validity of such a fit may be in doubt, and as a check, other criteria in addition to the accurate reproduction of the energy-level structure were used. The ground-state magnetic g values calculated from the fitted wave functions, $g_\parallel=0.5$ and $g_\perp=1.7$, were in good agreement with the experimental values, $g_\parallel=0.2(2)$ and $g_\perp=1.656(1)$.[21] Furthermore, the crystal-field parameters obtained from the fit were consistent with the parameters obtained for other rare-earth ions in $LuPO_4$,[22–26] as shown in Table II. Finally, the fitted spin-orbit-coupling parameter $\zeta_f=614$ cm^{-1} was only slightly smaller than the Ce^{3+} free-ion value[27] of 643.7 cm^{-1}—as expected for the atomiclike $4f$ configuration.

B. The first-excited configuration, $5d^1$

The $5d^1$ configuration of Ce^{3+} in YPO_4 (a crystal very similar to $LuPO_4$) has been studied by a number of workers using several different experimental techniques.[28–31] Disagreements exist in the literature regarding the energy-level assignments. For Ce^{3+} in $LuPO_4$ we observed seven broad spectral features between 30 000 and 50 000 cm^{-1}. An absorption spectrum taken in the liquid-helium temperature range is shown in Fig. 3. Features (a), (c)–(e), and (g) were identified as being the five electronic levels of the $5d^1$ configuration expected in D_{2d} symmetry. Feature (f) appeared in the absorption spectrum of pure $LuPO_4$,[32] indicating that it is from an impurity. A comparison of the absorption spectra of a nominally 20% Ce^{3+} in $LuPO_4$ crystal and a nominally 1% Ce^{3+} in $LuPO_4$ crystal showed that the strength of feature (b) is not correlated with the Ce^{3+} concentration, thus indicating that it is not due to a Ce^{3+} absorption.

Unlike the peaks in the $4f^N$-configuration spectra, the absorption features in the $5d^1$ spectrum showed no strong polarization characteristics. A high-resolution spectrum (liquid-helium temperature) of the lowest-energy absorption feature of a nominally 1% Ce^{3+} in

TABLE II. Hamiltonian parameters for various trivalent rare-earth ions in crystals of $LuPO_4$.

R^{3+}	x[a]	$4f^N$ ($N=$)	Crystal-field parameters (cm^{-1}) B_0^2	B_0^4	B_4^4	B_0^6	B_4^6	Spin-orbit parameters ζ (cm^{-1})	References
Ce	0.20	1	26	263	−1247	−1270	148	615	this work
Pr	b	2	21	280	−808	−1658	291	744	22
Nd	b	3	178	209	−922	−1256	−147	878	22
Eu	0.05	6	151	430	−820	−1263	272	1330	23
Tb	1.00	8	352	112	−800	−848	151		24
Er	b	11	146	69	−760	−643	−89	2367	25
Tm	b	12	203	117	−673	−705	16	2629	26
Yb	b	13	256	14	−608	−705[c]	16[c]	2903	26
Ce[d,e]	0.20	$5d^1$	3785	3968	−24 543			114	this work

[a]Nominal mole fraction.
[b]Approximately 0.01
[c]Fixed at Tm^{3+} values.
[d]Parameters for the Ce^{3+} $5d^1$ configuration.
[e]$F_0=41\,271$ cm^{-1} for the Ce^{3+} $5d^1$ configuration.

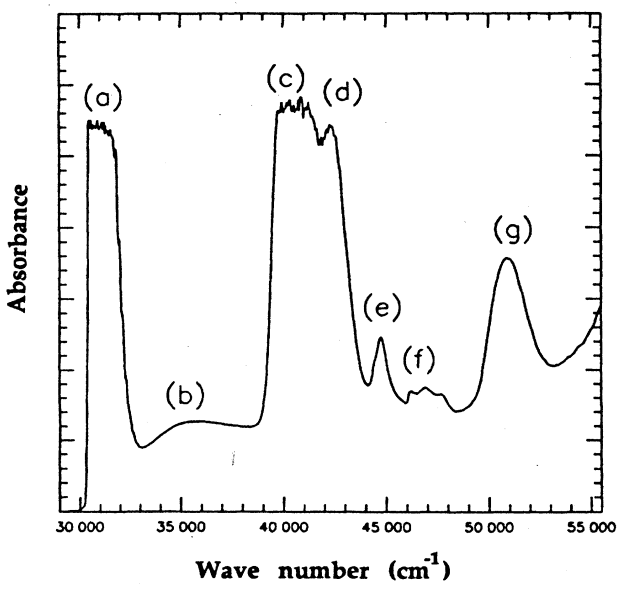

FIG. 3. Absorption spectrum of a nominally 20% Ce^{3+} in $LuPO_4$ crystal taken at 10 K. The peaks labeled (a), (c)–(e), and (g) are assigned to transitions to the states in the $5d^1$ configuration. Resolution was approximately 10–20 cm^{-1}. Peaks (b) and (f) are from impurities.

$LuPO_4$ crystal is shown in Fig. 4. A 1% Ce^{3+} crystal was used because the absorption from a 20% Ce^{3+} crystal was so strong that all detailed structure of the absorption peak was obscured. The sharp peak on the low-energy side was identified as the pure electronic-

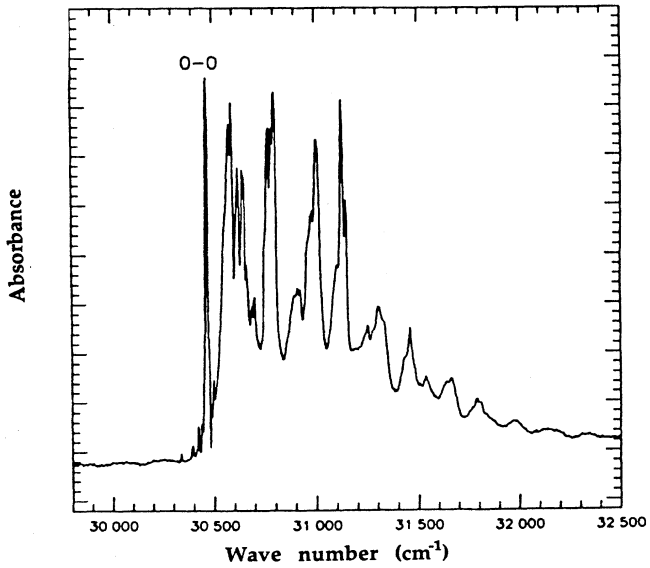

FIG. 4. Absorption spectrum of a nominally 1% Ce^{3+} in $LuPO_4$ crystal taken at 10 K. Only the transition to the lowest $5d^1$ level is shown. The resolution was approximately 1 cm^{-1}.

electronic or 0-0 transition from the ground state.[33] The other features superimposed on the broad peak were identified as transitions to vibronic states that result from the coupling between the lowest $5d^1$ electronic state and vibrational states of the lattice. These features have symmetries that are determined by both the nature of the electronic and vibrational states involved. The broad peak, which is a composite of vibronic states, did not show any uniform polarization characteristics. The symmetry of the electronic state can be determined from the polarization behavior of the 0-0 line. The 0-0 line for the lowest-energy feature was observed in both $\hat{\mathbf{Z}}$ and $\hat{\mathbf{Y}}$ polarizations. Using the electric dipole selection rules, for $\sigma=\hat{\mathbf{X}}$ and $\hat{\mathbf{Y}}$,

$$\Gamma_6\rightarrow\Gamma_6 \text{ or } \Gamma_7 ,$$
$$\Gamma_7\rightarrow\Gamma_6 \text{ or } \Gamma_7 , \tag{6}$$

and for $\pi=\hat{\mathbf{Z}}$,

$$\Gamma_6\rightarrow\Gamma_7 ,$$
$$\Gamma_7\rightarrow\Gamma_6 , \tag{7}$$

and the fact that the $4f^1$ ground state is a Γ_6 level, the lowest $5d^1$ level was assigned as a Γ_7 state. Unfortunately, the 0-0 lines for the four higher-energy features were not observed.

Even though the $5d^1$ states are considerably less "atomiclike" than the $4f^1$ states, a fit was made to a semiempirical Hamiltonian similar to that used previously for fitting the energy levels of the $4f^1$ configuration, i.e.,

$$H_{5d}=\zeta_{5d}(\boldsymbol{l}\cdot\mathbf{s})+(B_0^2)_{5d}C_0^2+(B_0^4)_{5d}C_0^4$$
$$+(B_4^4)_{5d}(C_4^4+C_{-4}^4)+F_0 , \tag{8}$$

where F_0 is the parameter fixing the mean energy of the $5d^1$ configuration relative to the lowest $4f^1$ level. The energies used in the fit were not at the absorption maxima, but rather were values on the low-energy sides of the absorption peaks where the 0-0 transitions are expected. The exact locations were estimated by assuming that for each level the shift from the maximum of the absorption was equivalent to the shift observed for the lowest level of the nominally 1% Ce^{3+} crystal. The wave functions resulting from the fit are fairly insensitive to the exact placement of the energy levels within the linewidths of the broad absorption peaks. Since only the symmetry of the lowest level was assigned experimentally, the symmetry assignments for the remaining four levels were made from the calculated energy levels. From group theory the remaining four electronic levels have to be assigned to two Γ_6 and two Γ_7 levels. This gives six possibilities for the remaining four assignments. The assignment that resulted in fitted crystal-field parameters with the same signs as the $4f^1$ crystal-field parameters was taken as correct. The values of the parameters obtained are given also in Table II. The wave functions are given in Table III. It can be seen from these results that the large crystal field has resulted in a significant amount of J mixing.

TABLE III. Wave functions for the $5d^1$ configuration of Ce^{3+} in crystals of nominally 20% Ce^{3+} in $LuPO_4$.

Energy (cm^{-1})	Symmetry	Wave function $\sum_{J,J_z} a(J,J_z)^{2S+1}L\|J,J_z\rangle$
30 468	Γ_7	$0.702\,^2D\|\frac{3}{2},-\frac{3}{2}\rangle+0.661\,^2D\|\frac{5}{2},\frac{5}{2}\rangle+0.266\,^2D\|\frac{5}{2},-\frac{3}{2}\rangle$
39 931	Γ_6	$0.953\,^2D\|\frac{3}{2},-\frac{1}{2}\rangle+0.304\,^2D\|\frac{5}{2},-\frac{1}{2}\rangle$
41 626	Γ_7	$-0.888\,^2D\|\frac{5}{2},-\frac{3}{2}\rangle+0.445\,^2D\|\frac{3}{2},-\frac{3}{2}\rangle-0.117\,^2D\|\frac{5}{2},\frac{5}{2}\rangle$
44 038	Γ_6	$0.953\,^2D\|\frac{5}{2},-\frac{1}{2}\rangle-0.304\,^2D\|\frac{3}{2},-\frac{1}{2}\rangle$
50 290	Γ_7	$-0.742\,^2D\|\frac{5}{2},\frac{5}{2}\rangle+0.556\,^2D\|\frac{3}{2},-\frac{3}{2}\rangle+0.376\,^2D\|\frac{5}{2},-\frac{3}{2}\rangle$

IV. INTENSITIES: NONRESONANT EXCITATION

A. Comparison with the standard calculation

An expression for the intensity of light (polarization ρ) scattered from an incident beam (polarization σ) by a Raman process may be written in terms of a scattering tensor element $\alpha_{\rho\sigma}$,[34]

$$\left[\frac{I_\rho}{\omega_s}\right] \propto \omega\omega_s^3|\alpha_{\rho\sigma}|^2\left[\frac{I_\sigma}{\omega}\right], \tag{9}$$

where ω and ω_s are the angular frequencies of the incident and scattered light, respectively. In the standard second-order theory, the scattering-tensor elements associated with an electronic Raman transition from an initial state $|i\rangle$ to a final state $|f\rangle$ are given by

$$(\alpha_{\rho\sigma})_{fi}=-\frac{1}{\hbar}\sum_r\left[\frac{\langle f|D_\rho|r\rangle\langle r|D_\sigma|i\rangle}{\omega_r-\omega}+\frac{\langle f|D_\sigma|r\rangle\langle r|D_\rho|i\rangle}{\omega_r+\omega_s}\right], \tag{10}$$

where $\mathbf{D}$ denotes the electric dipole operator, and $\hbar\omega_r$ is the energy of the virtual intermediate state $|r\rangle$. The sum is over the states $|r\rangle$ belonging to excited configurations with parity opposite that of the ground configuration.

If the energy denominators in Eq. (10) are assumed to be constant for all states in a given excited configuration, then closure may be performed over the angular variables for that configuration. This process is facilitated by use of spherical tensor operators. The results of such a calculation are given in terms of the spherical scattering-tensor elements α_Q^K, where $K=1,2$ and $Q=-K,-K+1,\ldots,K$. The angular parts of the initial- and final-state wave functions are written as

$$\Psi_i=\sum_{J,J_z} a(i;S,L,J,J_z)|S,L,J,J_z\rangle\ . \tag{11}$$

α_Q^K is then given by[35]

$$(\alpha_Q^K)_{fi}=F(K,\omega)\sum_{S,L,J,J_z}\sum_{S',L',J',J_z'} a^*(i;S,L,J,J_z)a(f;S',L',J',J_z')\langle S',L',J',J_z'|U_Q^K|S,L,J,J_z\rangle\ , \tag{12}$$

where U_Q^K is the spherical unit tensor. $F(K,\omega)$ is dependent on the radial wave functions of the ground and excited configurations and the average energies of the excited configurations:

$$F(K,\omega)=\frac{(-1)^K}{\hbar}\sum_{4f^{N-1}n'l'}\left[\frac{1}{\bar\omega_{n'l'}-\omega}+(-1)^K\frac{1}{\bar\omega_{n'l'}+\omega}\right]\langle 3\|c^{(1)}\|l'\rangle^2\langle 4f|r|n'l'\rangle^2(2K+1)^{1/2}\begin{Bmatrix}1 & K & 1\\ 3 & l' & 3\end{Bmatrix}, \tag{13}$$

where $\hbar\bar\omega_{n'l'}$ is the average energy of the excited configuration $4f^{N-1}n'l'$.

The unit-tensor matrix elements are easily evaluated. The Cartesian scattering-tensor elements $\alpha_{\rho\sigma}$ may be written as linear combinations of the spherical tensors.[20,36] Since each energy level is actually a Kramers doublet, then each observed intensity is associated with the four transitions between individual Kramers levels. The scattering-tensor elements for each of these transitions are computed separately, squared, and then added together to obtain the total scattering intensity.

$F(1,\omega)$ and $F(2,\omega)$ cannot be computed directly unless the radial wave functions and energies of the opposite-parity configurations are known. The relative scattering

intensities are, however, dependent only on the ratio, $[F(1,\omega)/F(2,\omega)]^2$. If one assumes that only states from the lowest-energy configuration $4f^{N-1}5d^1$ are important in mediating the electronic Raman scattering process, then from Eq. (13) we have

$$\frac{F(1,\omega)}{F(2,\omega)}=1.3\frac{\omega}{\bar{\omega}_{5d}} . \tag{14}$$

For the nonresonant experiment, $\omega/2\pi c \approx 20\,000$ cm^{-1} and $\bar{\omega}_{5d}/2\pi c \approx 40\,000$ cm^{-1}—resulting in a value for $F(1,\omega)/F(2,\omega)$ of 0.65.

The calculated values $[F(1,\omega)/F(2,\omega)=0.65]$ for the squared scattering-tensor elements are compared to the values derived from the observed electronic spectra in Fig. 5. The observed values were obtained by measuring the area under the Raman peaks, and scaling each of these values by the appropriate values of $1/\omega_s^3$ and by factors correcting for the frequency response of the detection system. The observed and calculated values were finally scaled relative to each other by averaging the observed-to-calculated ratios for all transitions with nonzero intensity. As can be seen, the agreement is poor.

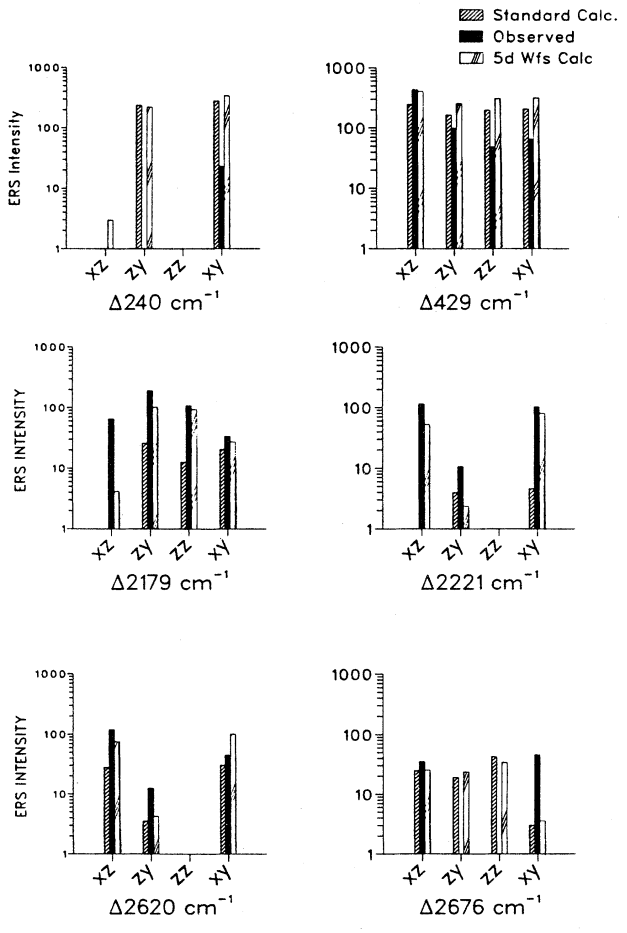

FIG. 5. The observed electronic Raman transition intensities for a nominally 20% Ce^{3+} in $LuPO_4$ crystal and the intensities calculated using either the standard second-order theory or by explicit evaluation of the sum over intermediate states.

The largest discrepancies exist for the transitions to the levels at 240 and 2676 cm^{-1}, for which the calculated intensities are much larger than the observed intensities. In addition, the calculation underestimates the strengths of the transitions to the 2179-, 2221-, and 2620-cm^{-1} levels relative to the transition to the 429-cm^{-1} level. The higher-energy levels all belong to the $^2F_{7/2}$ multiplet, while the 429-cm^{-1} level belongs to the $^2F_{5/2}$ multiplet. Thus the standard theory underestimates the strength of the $^2F_{5/2}\rightarrow{}^2F_{7/2}$ scattering relative to the $^2F_{5/2}\rightarrow{}^2F_{5/2}$ scattering. This is clearly demonstrated in Table IV, which shows the measured and calculated values for the ratio of the intensity of the $^2F_{5/2}\rightarrow{}^2F_{5/2}$ and $^2F_{5/2}\rightarrow{}^2F_{7/2}$ scattering. The reason for the large difference in the calculated intensities for the transitions to the two multiplets can be seen directly from the respective values for the reduced matrix elements of the spherical tensor operators: For $^2F_{5/2}\rightarrow{}^2F_{5/2}$,

$$\begin{aligned}\langle L',S',J'\|U^1\|L,S,J\rangle&=0.903 ,\\ \langle L',S',J'\|U^2\|L,S,J\rangle&=0.857 ,\end{aligned} \tag{15}$$

and for $^2F_{5/2}\rightarrow{}^2F_{7/2}$,

$$\begin{aligned}\langle L',S',J'\|U^1\|L,S,J\rangle&=0.202 ,\\ \langle L',S',J'\|U^2\|L,S,J\rangle&=0.350 .\end{aligned} \tag{16}$$

It is possible that a different value of $F(1,\omega)/F(2,\omega)$ might fit the data more suitably. Becker *et al.*[8] found for electronic Raman scattering from $TmPO_4$ that a value of $F(1,\omega)/F(2,\omega)=-0.03$ fitted the experimental data much better than the value $F(1,\omega)/F(2,\omega)=0.25$. The latter value was calculated based on the assumption that the intermediate states were from the $4f^{N-1}5d$ configuration alone. The small value for $F(1,\omega)/F(2,\omega)$ was later interpreted as indicating that the *g* orbitals were just as important in mediating the electronic Raman process as the *d* orbitals. This somewhat surprising suggestion (considering the relative energies of $4f^{N-1}n'd$ orbitals and $4f^{N-1}n'g$ orbitals in the free ion) has also been used in the interpretation of intensities of one-photon processes in rare-earth-doped crystals.[37–39] A sensitive test of the value of $F(1,\omega)/F(2,\omega)$ is the predicted value of the change in intensity that results when the polariza-

TABLE IV. Measured and calculated ratios of the electronic Raman multiplet-to-multiplet intensities. Intensity for $^2F_{5/2}\rightarrow{}^2F_{5/2}$ includes transitions from the ground state to the levels at 240 and 429 cm^{-1}. Intensity for $^2F_{5/2}\rightarrow{}^2F_{7/2}$ includes the transitions from the ground state to the levels at 2179, 2221, 2620, and 2676 cm^{-1}.

	Measured	Calc. closure approx. $\frac{F(1,\omega)}{F(2,\omega)}=0.65$	Calc. explicit
$\frac{^2F_{5/2}\rightarrow{}^2F_{5/2}}{^2F_{5/2}\rightarrow{}^2F_{7/2}}$	0.8	6.1	2.9

tions of the incident photon and the scattered photon are interchanged. The scattering asymmetry is defined as the ratio (I_{XZ}/I_{ZX}). Table V lists the observed scattering asymmetries and the scattering asymmetries that were calculated using a value of $F(1,\omega)/F(2,\omega)=0.65$. The agreement between the measured and calculated values is poor. This is particularly evident for the transition to the 2221-cm^{-1} level. In order to find a value of $F(1,\omega)/F(2,\omega)$ that might represent a better fit of the data, we equated the theoretical expressions describing the scattering asymmetries with the observed values of the asymmetries and solved for $F(1,\omega)/F(2,\omega)$ in each case. Table VI lists the observed scattering asymmetries and the derived values of $F(1,\omega)/F(2,\omega)$. For each transition there are two derived values for $F(1,\omega)/F(2,\omega)$ because the expressions describing the asymmetries are quadratic in this quantity. The value of $F(1,\omega)/F(2,\omega)$ should be independent of the particular $4f^1$ states involved in the transition. No consistent value for $F(1,\omega)/F(2,\omega)$ appears, however.

Thus it appears that the standard second-order calculation is insufficient to explain the data. This result is not surprising considering how close the onset of the $5d^1$ configuration is to the incident laser energy (10 000 cm^{-1}) compared to the $5d^1$ configuration's overall breadth (20 000 cm^{-1}). The detailed structure of the $5d^1$ configuration should be of importance.

B. Comparison with the explicit calculation

More detailed properties of the intermediate-state structure may be considered by the addition of higher-order perturbation terms in the expression for the scattering amplitude.[7] In the present work the excited configuration has been observed spectroscopically. A crystal-field fit has been performed, and the angular parts of the wave functions for the states of the configuration are available. There are only five Kramers doublets, and the $5d^1$ states and their energies have been used explicitly in the summation of Eq. (10). It is not clearly evident whether the energies of the 0-0 lines or the energies of the absorption maxima should be used in the denominator of Eq. (10). For the nonresonant excitation at 19 429.7 cm^{-1} there is very little difference between the intensities calculated using the 0-0 energies and the absorption-maxima energies. For resonant excitation at 28 191.5 cm^{-1}, however, there is a difference which will be discussed in the following section.

The result of a calculation using the 0-0 energies, as compared to the data, is also shown in Fig. 5. The scaling between the data and the calculated results was done as before for the standard second-order calculation.

The agreement is improved over the results based on the closure approximation. Most notably, the problem of the relative intensities of the $^2F_{5/2}\rightarrow{}^2F_{5/2}$ transitions to the $^2F_{5/2}\rightarrow{}^2F_{7/2}$ transitions has been somewhat rectified. The improvement can be seen from the ratios displayed in Table IV. In addition, the explicit calculation more accurately describes the observed scattering asymmetries (Table V). Unfortunately, the explicit calculation still fails to predict accurately scattering intensities for the 240- and 2676-cm^{-1} levels.

TABLE V. Measured and calculated scattering asymmetries. For the transition to the 240-cm^{-1} level, no scattering was observed for both the $\hat{\mathbf{X}}\hat{\mathbf{Z}}$ and $\hat{\mathbf{Z}}\hat{\mathbf{Y}}$ polarizations. For the transition to the 2676-cm^{-1} level, no scattering was observed in the $\hat{\mathbf{Z}}\hat{\mathbf{Y}}$ polarization.

Transition (cm^{-1})	Measured	Scattering asymmetry Calc. closure approx. $\frac{F(1,\omega)}{F(2,\omega)}=0.65$	Calc. explicit
240		0.0002	0.013
429	4.3	1.5	1.6
2179	0.34	0.01	0.04
2221	10.9	0.09	22.2
2620	9.5	7.9	18.0
2676	large	1.1	1.1

TABLE VI. Values of $F(1,\omega)/F(2,\omega)$ calculated from the observed scattering asymmetries. The expression for the scattering asymmetry is quadratic in $F(1,\omega)/F(2,\omega)$, so that two values of $F(1,\omega)/F(2,\omega)$ are possible.

Transition Δ (cm^{-1})	Calculated values $\frac{F(1,\omega)}{F(2,\omega)}$
240	a
429	2.26 or 18.5
2179	0.14 or 1.95
2221	−0.19 or −0.66
2620	0.71 or 2.74
2676	10.3

[a]Both $I_{XZ}=I_{ZY}=0$.

V. NEAR-RESONANT EXCITATION

An order-of-magnitude estimate of the expected enhancement of the electronic Raman scattering intensity excited by the frequency-tripled output of a Nd^{3+}:YAG laser at 355 nm (28 191.5 cm^{-1}) relative to that excited by the argon-ion laser at 514.5 nm (19 429.7 cm^{-1}) is given by

$$\left[\frac{\omega_{5d}-\omega_{514.5}}{\omega_{5d}-\omega_{355.0}}\right]^2\approx 25\ , \tag{17}$$

where the enhancement resulting from the ω^4-type scattering dependence (which results in an additional enhancement factor of approximately 4.5) has not been included. This calculation assumes that the major electronic Raman scattering intensity is mediated through the states of the $5d^1$ configuration. A comparison of the actual enhancements to this estimated number should serve as a test of the assumption.

The observed electronic Raman scattering intensities for the lines at 429, 2179, 2221, and 2620 cm^{-1} from laser excitation at both 514.5 and 355 nm are shown in Fig. 6.

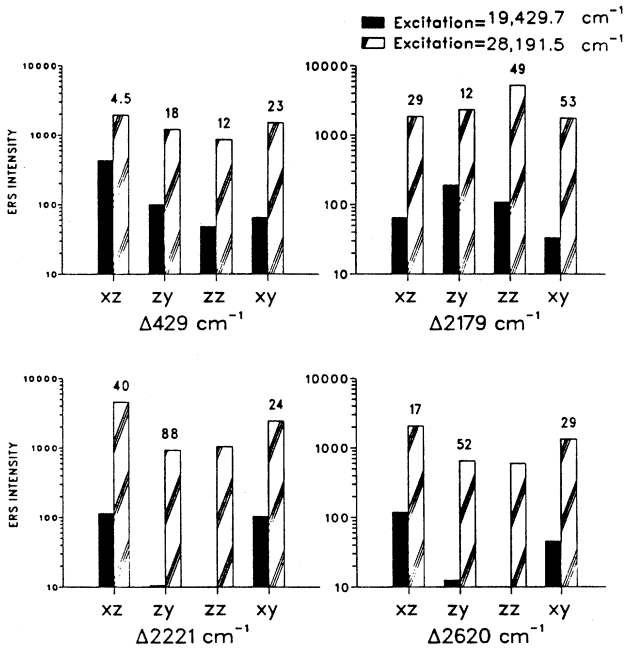

FIG. 6. Intensities of electronic Raman transitions for a nominally 20% Ce^{3+} in $LuPO_4$ crystal excited with the 514.5-nm line of an argon-ion laser and the frequency-tripled output of a Nd^{3+}:YAG laser (355 nm). The numbers above the bars indicate the resonance-enhancement ratios.

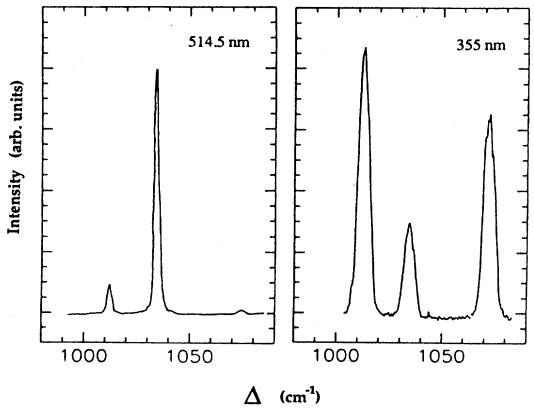

FIG. 7. Raman spectra of a nominally 20% Ce^{3+} in $LuPO_4$ crystal showing the phonon in the range 1000–1050 cm^{-1}. Spectrum *A* was excited by 514.5-nm light. Spectrum *B* was excited by 355-nm light. The polarization is $\hat{X}\hat{Z}$.

The lines at 240 and 2676 cm^{-1} were not observed. As described previously, the data have been normalized using the 1034-cm^{-1} E_g phonon of the crystal, correcting for experimental variations and the ω^4-type scattering dependence. The enhancement ratios are also shown. For the observed lines, the enhancement ratios indicate that, indeed, the $5d^1$ configuration plays a major role as an intermediate channel. The only unexpected result is that some of the transitions show anomalously large enhancements. For example, the $\hat{Z}\hat{Y}$-polarized transition to the 2221-cm^{-1} level shows an enhancement of approximately 100.

The anomalously large enhancements are probably the result of polarization leakage caused by actual physical damage to the crystal as a result of irradiation by the tripled Nd^{3+}:YAG output. After such irradiation, anomalies in the polarized-phonon Raman spectra can be observed that were not present before the 355-nm irradiation. Above a certain threshold intensity, the crystal is visibly damaged although the polarization anomalies are present even below the visible damage threshold. The $\hat{X}\hat{Z}$ Raman spectrum of a nominally 20% Ce^{3+} in $LuPO_4$ crystal is shown in Fig. 7 with two excitation frequencies, 514.5 and 355 nm. The lower-frequency excitation spectrum was obtained first. The A_{1g} phonon at 1013 cm^{-1}, although weakly present at 514.5 nm, should not be allowed in this polarization combination, but is the strongest transition in the 355-nm excitation spectrum. The loss of polarization selection rules is found for all polarization combinations after irradiation. The breakdown of the selection rules seems to be more characteristic in the phonon Raman spectra than in the electronic Raman spectra. The 355-nm excited spectra for the 2179- and 2221-cm^{-1} transitions are shown in Fig. 8. In the electronic Raman spectra, the forbidden $\hat{Z}\hat{Z}$ transitions are still smaller, in general, than the allowed transitions. This difference may reflect the fact that the phonons tend to be excitations of the lattice, while the rare-earth-ion electronic states are more localized in nature. Thus the phonons are more sensitive to structural changes.

The $5d^1$ wave functions and energies can be used to calculate explicitly the expected intensities from near-resonant excitation. Two calculations were performed, one with the 0-0 energies of the $5d^1$ states in the energy denominator of Eq. (10), and the second with the absorption maxima in this denominator. The calculation using

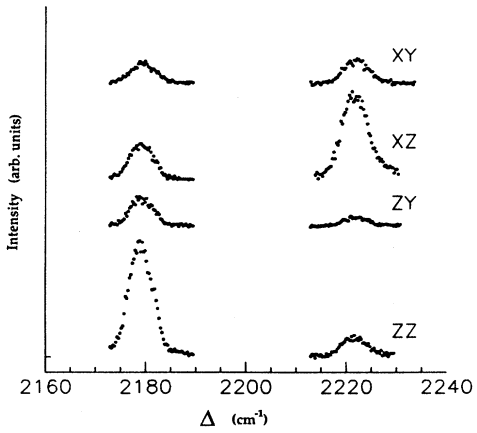

FIG. 8. Electronic Raman spectrum of a nominally 20% Ce^{3+} in $LuPO_4$ crystal excited by 355-nm light. The temperature was ≈ 10 K.

the absorption maxima as the energy denominators resulted in intensities that were approximately 65% of the intensities calculated using the 0-0 energies. This difference is primarily due to the scaling of the energy denominator in Eq. (10) by the change in $\omega_r - \omega$ for the lowest $5d^1$ energy level. The only exceptions involved the transitions to the Γ_7 final states in which the incident laser photons were polarized along the $\hat{Z}$ axis. In these instances there was no substantial difference between the two calculations because the lowest-energy $5d^1$ state does not act as a virtual intermediate state. Neither of these two calculations is completely accurate, but they do show approximate upper and lower bounds to the electronic Raman intensities.

A comparison of the observed and calculated intensities (using 0-0 energies) from excitation at 355 nm is shown in Fig. 9. The calculation is the same as for the nonresonant case, except for the change in the energy denominators. The measured and calculated intensities are scaled relative to each other with the same factor used earlier for scaling the nonresonant result. Thus, the scale in Fig. 9 is equivalent to the scale in Fig. 5.

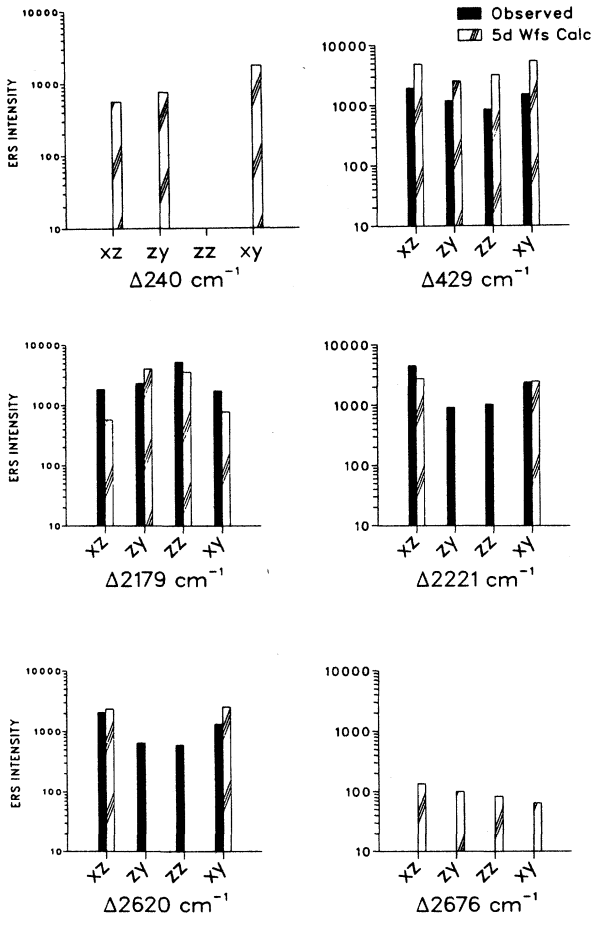

FIG. 9. The observed intensities of electronic Raman scattering from a nominally 20% Ce^{3+} in $LuPO_4$ crystal excited by 355-nm light, and values calculated by explicit evaluation of the sum over the states of the $5d^1$ configuration. Scale is the same as Fig. 5.

TABLE VII. Polarization-averaged, relative electronic Raman scattering intensities for spectra excited using 355-nm radiation.

Transition (cm^{-1})	Intensities Measured	Calc. explicit
240	0	1543
429	2738	8008
2179	5591	4514
2221	4462	2913
2620	2315	2447
2676	0	193

The loss of the integrity of the polarization makes it difficult to compare the results in a very precise manner. The polarization loss is apparent in considering the different polarization combinations for any given transition. While the calculated values sometimes show large differences between different polarizations, the observed values show a smooth variation, suggesting that intensity was redistributed from one polarization to another. The main feature to note is that the calculation seems to predict fairly accurately the overall signal level for the observed transitions, even if it does not predict the relative intensities between different polarization combinations. This result is demonstrated in Table VII, which shows the measured and calculated polarization-averaged relative intensities of the electronic Raman transitions. The agreement is good, but there are a few notable discrepancies between the measured and calculated intensities. For example, as in the case of the nonresonant experiment, the calculation overestimates the scattering to the $^2F_{5/2}$ levels relative to that of the $^2F_{7/2}$ levels. In addition, there is again some difficulty with the transitions to the levels at 240 and 2676 cm^{-1}. Neither of these levels are observed, even with the benefit of resonant enhancement. It should be noted, however, that the detection limit of the 355-nm experiment is approximately 50 times smaller than that of the 514.5-nm case. This places the detection limit at approximately 500 on the present scale. This could explain the absence of observed scattering to the 2676-cm^{-1} level, but not to the 240-cm^{-1} level.

VI. CONCLUSIONS

Comparison of the nonresonantly excited electronic Raman scattering intensities from Ce^{3+} doped into $LuPO_4$ with the intensities predicted by the standard second-order theory of two-photon processes in rare-earth ions shows that the theory is inadequate. This disagreement is attributed to the low relative energy of the states of the $5d^1$ configuration of Ce^{3+}, which invalidates the closure approximation. A second calculation

was carried out by explicitly evaluating the sum over the intermediate states using the observed energies and crystal-field-fit wave functions of the $5d^1$ configuration. This calculation described the observed scattering intensities more accurately, indicating that the states of the $5d^1$ configuration serve as the dominant intermediate channels for electronic Raman scattering in this crystal. For this system, configurations of the type $4f^{N-1}g$ as the intermediate states appear to play no significant role.

In addition, the electronic Raman spectra exhibited intensity enhancements on the order of 100 (including the enhancement due to the ω^4 scattering dependence) when the laser excitation was tuned close to the $5d^1$ configuration. Such an enhancement is in agreement with the predictions of the explicit calculation and further supports the assumption that the states of the $5d^1$ configuration serve as the dominant intermediate states for Ce^{3+}.

ACKNOWLEDGMENTS

We are deeply indebted to J. A. Koningstein for helpful discussions during his visits to our laboratory. We thank Shangda Xia and Richard Leavitt for contributing many suggestions that have helped with the analysis of the data. We also acknowledge the efforts of J. J. Bucher and R. E. Russo during the whole course of this research effort. Finally, we would like to thank D. Piehler and D. S. Kim for letting us use their results for the crystal-field fit for Eu^{3+}:$LuPO_4$. This research was supported in part by the Director, Office of Energy Research, Office of Basic Energy Sciences, Chemical Science Division, the U.S. Department of Energy, under Contract No. DE-AC03-76SF00098. Oak Ridge National Laboratory is operated by Martin Marietta Energy Systems Inc., for the U.S. Department of Energy, under Contract No. DE-AC05-84OR21400.

*Present address: Naval Research Laboratory, Washington, D.C. 20375-5000.

†Present address: AT&T Bell Laboratories, Murray Hill, NJ 07974-2070.

[1]J. D. Axe, Phys. Rev. **136A**, 42 (1964).

[2]B. R. Judd, Phys. Rev. **127**, 750 (1962).

[3]G. S. Ofelt, J. Chem. Phys. **37**, 511 (1962).

[4]M. Dagenais, M. Downer, R. Neumann, and N. Bloembergen, Phys. Rev. Lett. **46**, 561 (1981).

[5]M. C. Downer, A. Bivas, and N. Bloembergen, Opt. Commun. **41**, 355 (1982).

[6]M. C. Downer and A. Bivas, Phys. Rev. B **28**, 3677 (1983).

[7]B. R. Judd and D. R. Pooler, J. Phys. C **15**, 591 (1982).

[8]P. C. Becker, N. Edelstein, G. M. Williams, J. J. Bucher, R. E. Russo, J. A. Koningstein, L. A. Boatner, and M. M. Abraham, Phys. Rev. B **31**, 8102 (1985).

[9]P. C. Becker, N. Edelstein, B. R. Judd, R. C. Leavitt, and G. M. S. Lister, J. Phys. C **18**, L1063 (1985).

[10]L. L. Chase and S. A. Payne, Phys. Rev. B **34**, 8883 (1986).

[11]R. L. Wadsack and R. K. Chang, Solid State Commun. **10**, 45 (1972).

[12]D. Nicollin and J. A. Koningstein, Chem. Phys. **49**, 377 (1980).

[13]P. Myslynski and J. A. Koningstein, Chem. Phys. **114**, 137 (1987).

[14]P. C. Becker, G. M. Williams, R. E. Russo, N. Edelstein, J. A. Koningstein, L. A. Boatner, and M. M. Abraham, Opt. Lett. **11**, 282 (1986).

[15]G. M. Williams, P. C. Becker, N. Edelstein, L. A. Boatner, and M. M. Abraham, Phys. Rev. B **40**, 1288 (1989).

[16]E. Nakazawa and F. Shiga, J. Lumin. **15**, 255 (1977).

[17]W. O. Milligan, D. F. Mullica, G. W. Beall, and L. A. Boatner, Inorg. Chim. Acta **60**, 39 (1982).

[18]The actual amount of Ce^{3+} in the single crystals was later found to be much less than the starting proportion. G. M. Williams *et al.*, this issue, the following paper, Phys. Rev. B **40**, 4143 (1989).

[19]E. Nakazawa and S. Shinoya, J. Phys. Soc. Jpn. **36**, 504 (1974).

[20]J. A. Koningstein, *Introduction to the Theory of the Raman Effect* (Reidel, Dordrecht, 1972).

[21]M. M. Abraham, L. A. Boatner, J. O. Ramey, and M. Rappaz, J. Chem. Phys. **78**, 3 (1983).

[22]T. Hayhurst, G. Shalimoff, J. G. Conway, N. Edelstein, L. A. Boatner, and M. M. Abraham, J. Chem. Phys. **76**, 3960 (1982).

[23]D. Piehler and D. S. Kim (private communication).

[24]Marie-France Joubert, Ph.D. thesis, l'Universitié Claude-Bernard–Lyon 1, 1986.

[25]T. Hayhurst, G. Shalimoff, N. Edelstein, L. A. Boatner, and M. M. Abraham, J. Chem. Phys. **74**, 5449 (1981).

[26]P. C. Becker, T. Hayhurst, G. Shalimoff, J. G. Conway, N. Edelstein, L. A. Boatner, and M. M. Abraham, J. Chem. Phys. **81**, 2872 (1984).

[27]Brian G. Wybourne, *Spectroscopic Properties of Rare Earths* (Wiley, New York, 1965).

[28]G. Blasse and A. Bril, J. Chem. Phys. **47**, 5139 (1967).

[29]J. P. Briffaut and J. P. Denis, Phys. Status. Solidi **41**, 781 (1970).

[30]R. C. Naik and N. P. Karanjikar, Technical Report, Bhabha Atomic Research Center, Bombay, India, 1982 (unpublished).

[31]G. Balasubramanian and D. J. Newman, J. Phys. Chem. Solids **36**, 57 (1975).

[32]Glen M. Williams, Ph.D. thesis, University of California, Berkeley, 1988.

[33]Indications are that the 0-0 line for the nominally 20% Ce^{3+} in $LuPO_4$ crystal is approximately 200 cm^{-1} lower in energy than the 0-0 line of the nominally 1% Ce^{3+} in $LuPO_4$ crystal. However, this has no significant effect on our calculations.

[34]R. Loudon, *The Quantum Theory of Light* (Clarendon, Oxford, 1983).

[35]O. S. Mortensen and J. A. Koningstein, J. Chem. Phys. **48**, 3971 (1968).

[36]The scattering tensors were rotated by 45° about the $\hat{\mathbf{Z}}$ axis, so that the tensors were expressed in terms of the crystallographic axes, which are rotated by 45° relative to the Ce^{3+} local axes. See Ref. 8.

[37]W. F. Krupke, Phys. Rev. **145**, 325 (1966).

[38]P. J. Becker, Phys. Status Solidi B **43**, 583 (1971).

[39]M. Hasunama, K. Okada, and Y. Kato, Bull. Chem. Soc. Jpn. **57**, 3036 (1974).